Peer Review File

Manuscript Title: Chiral Assemblies of Pinwheel Superlattices on Substrates

Reviewer Comments & Author Rebuttals

Reviewer Reports on the Initial Version:

Referee expertise:

Referee #1: chiral nanoparticles

Referee #2: nanomaterials, colloids and self-assembly

Referee #3: self-assembly

Referees' comments:

Referee #1 (Remarks to the Author):

This is a very nice study, demonstrating the self-assembly of Au tetrahedral nanocrystals into (a)chiral structures on a solid support. The work was carefully conducted, and it was also supported by nice optical measurements, in situ LCTEM observation, and computational simulation. I would like to see this work published as soon as possible to enhance the community's interest in using this approach for the fabrication of metamaterials for applications in the visible region. Here are some general comments that should be addressed during the revision of this manuscript:

1) Since the tetrahedral building blocks could be chiral too if the are not perfect tetrahedra (e.g., the corners might have different degrees of truncation or the distribution of the CTAB bilayers are not uniform across the surface). Would this affect the optical measurements?

2) For a CTAB-based system, it is well known that the bilayer might be disrupted due to desorption of the surfactant molecules during sample preparation, such as drying/washing of the sample. Would this affect the outcome of the assembly process?

3) How large can the self-assembled structures be? what is the limit of the vertical thickness?

4) A more quantitative measure of the water evaporation and self-assembly process would be helpful. Right now, it was stated that the evaporation was controlled by pressing the petri dish, which seems to be vague to me.

Referee #2 (Remarks to the Author):

Nature manuscript 2022-04-06804
Chiral Assemblies of Pinwheel Superlattices on Substrates
by S. Zhou et al.
I very much enjoyed reading this manuscript. The demonstrated fabrication of chiral lattices of tetragonal gold nanoparticles is very exciting as they can pave the way to unprecedented applications. The combination of nanophotonic/nanoplasmonic properties with chirality-induced optical activity is potentially very promising. The authors have presented convincing experimental data using various techniques, which are further supported by simulations.
As far as I understand, each nanoparticle cluster has a well-defined sense of handedness while the whole ensemble is racemic, isn’t it? Is there a way to push the system to a particular side during

the symmetry breaking? Can one potentially try using chiral surfactants or apply an external perturbation such as circularly-polarized light? I would appreciate a short discussion of this point.
As pointed by the authors, single-layer structures become chiral due to the presence of the substrate. Did the authors attempt to use different substrate materials to demonstrate the substrate influence experimentally, for example in optical activity?
On line 88 the authors quote the strength of face-to-face nanoparticle repulsion of 0.59 kBT. Where does this number come from? I did not find it in the supplementary or the main text. By the way, add a space between the number and the "unit" (kBT).
On line 92 the authors use two times the van der Waals energy symbol with the subscript "vdW" and "vdw". Use consistent notations.
Line 60 "experimentally realization" -> experimental realization?
Andrei V. Petukhov

Referee #3 (Remarks to the Author):

Tetrahedral building blocks are known to be able to be packed into fertile and complex superstructural polymorphs. In this report, the authors achieved a previously unknown (at least to my knowledge) so-called pinwheel structure from tetrahedral gold nanocrystals. One of the remarkable findings is that the pinwheel lattices break structural symmetries, thereby leading to the unique chiral optical response which is experimentally confirmed by the photon-induced near-field electron microscopy (PINEM). In addition, the optical chirality can be tuned by controlling the assembly conditions (particle sizes, superlattice domains, solution ionic strength) to balance the two major inter-particle interactions of the system: van der Waals attraction and electrostatic repulsion. Both experimental data with detailed analyses, and high level of calculation/modeling results are provided to coherently support their claims and conclusions. I feel that this paper presents an innovative experimental demonstration of compelling chiral optical properties arising from unique nanoarchitectures, which is important to the fields of nano-assemblies, optoelectronics, spintronics, and metamaterials. Overall, I support this paper for publication in Nature and believe that the discovery will fill some gaps between nanocrystal-based chiral-type assemblies and functional solid materials with intriguing properties.

1. Through reading the paper, I do not quite feel that using the terms of "perovskite" are necessary or even accurate. Normally, perovskite structure retains its octahedral corner connection point during deformation or transformation, which is clearly not the case in this paper. As much as I value this paper, it may not be appropriate to use a buzzword like "perovskite" to show its significance.

2. As I see in Figure 2b-d, it is unclear whether the structure hold the corner-to-corner or face-to-face connection between the neighboring building blocks. It is confusing to me how do the authors define the corner-to-corner or the corner-to-edge superlattices? Is this defined based on the distance? For the corner-to-corner lattice (honeycomb structure), is the distance between two connected corners significantly smaller than that between the two registered faces? How about the corner-to-edge structure?

3. Authors claimed that the tetrahedral gold nanocrystals used in this study are coated with both CTAB (on the faces) and thiol (on the corners), but I donot find the synthetic details about how the authors achieve this asymmetric ligand coverage. Authors should also provide direct evidence to show there are indeed two types of ligands on the particle surfaces. In addition, it is known that the ligand coating on the shaped metal nanocrystals is not uniform (less dense on the corners than on the face), which may play roles when considering the interparticle interactions. Do authors consider this effect? For example, if there is no thiol ligand coverage on the corner, is the structure trapped in the corner-sharing honeycomb structure?

4. When the pinwheel structure is formed and evolved, do the faces of neighboring tetrahedra

remain parallel? How about the registration area change between the two touching faces during the process? I would imagine the area should be getting smaller during the “compression” process, which in turn alters the interparticle interactions (for both electrostatic repulsion and van der Waals attraction). Can the authors comment on it?

5. I would like to see more detailed characterizations of the tetrahedral gold nanocrystals (after depletion purification) used for assemblies. TEM and SEM images for large area survey and individual particles with statistical analyses of the particle geometry should be provided. I do not question the size and shape determined by the authors, but I would appreciate if the authors could provide these raw data to the readers.

6. The authors mentioned the importance of the domain size to the materials’ chiral properties, I am curious about the maximum domain size of the pinwheel superlattices that the authors obtained using this method?

7. According to the description at the line 101-102, "the effective "compression" increases the packing fraction to 2/3 when all tetrahedra rotate in-plane by 30°." More clarification of this sentence is needed. Having seen chiral assemblies like Figure 3c, or Figure 2e, I find it is difficult to believe that the chiral structure (looks like a more opened structure) is actually compressed and has a doubled packing density as compared to the original honeycomb structure.

8. The origin of the chirality, as described in lines 104-108, does not quite make sense to me. Do you know other examples of chirality arising only when the structure is deposited on a substrate (if so, the works should be cited). It would be helpful if the authors can provide some schematic drawings to show this. Is this because of the fixed structure orientation (viewing direction) after sitting on a substrate or different assembly behavior when substrate is presence? Also, in line 107, I donot understand what do the authors mean by “flipping results into an inequivalent mirror image”. What is this “inequivalent mirror image?” More explanation and experimental results are needed.

Author Rebuttals to Initial Comments:

Responses to Reviewer 1

Reviewer 1 considered our work positively as "*carefully conducted, and it was also supported by nice optical measurements, in situ LCTEM observation, and computational simulation*", and "*would like to see this work published as soon as possible to enhance the community's interest in using this approach*". We thank the reviewer for the great comments, all of which we have now addressed with new experiments (new Supplementary Figs. 1d, 2c–g, 3a–f, 8a,b, 24, and 27), new analysis, and new finite-difference time-domain (FDTD) simulations (new Supplementary Fig. 17h–u), particularly on identifying the effect of uneven truncation for tetrahedral building blocks, disrupting cetyltrimethylammonium bromide (CTAB) bilayers, and quantifying the assembly conditions.

Comment 1: *Since the tetrahedral building blocks could be chiral too if they are not perfect tetrahedra (e.g., the corners might have different degrees of truncation or the distribution of the CTAB bilayers are not uniform across the surface). Would this affect the optical measurements?*

Reply: We thank the reviewer for the insightful comment.

In the revised manuscript, we have added the following new experimental data and new analysis to show that there is no significant uneven truncation or ligand-induced chirality in the nanoparticles (NPs). We also used new FDTD simulation to show that even when "chiral" corner truncation is present, the assembled structure's circular dichroism (CD) spectrum is not affected, suggesting that our observed chiroptical activity is a collective effect of the ensemble superlattice.

1. We analyzed the extent of truncation for the small, middle, and large-sized tetrahedra (100 each), and identified that the corner truncation of all the samples has a narrow, single-peaked distribution on the single NP level (the new Supplementary Fig. 2c–g). We added details of this measurement in Supplementary Notes 1 and 2.

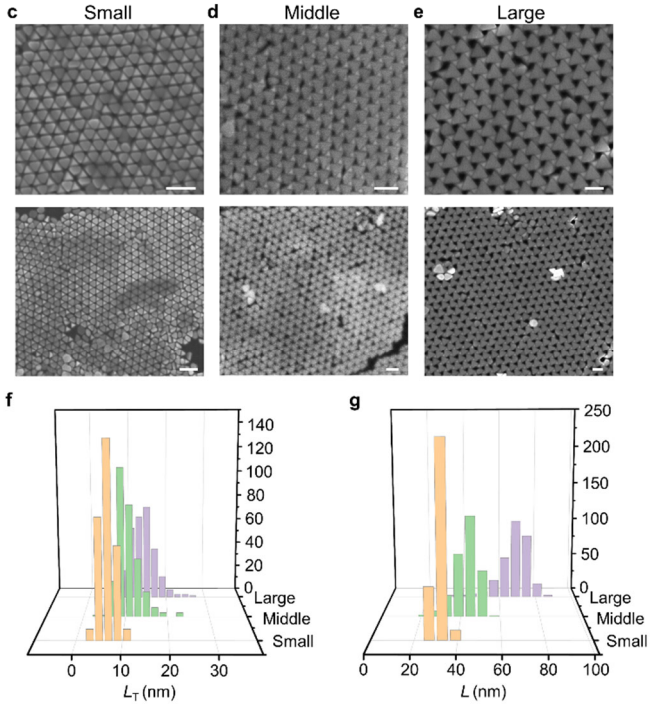

Supplementary Fig. 2c–g. (**c**–**e**) Representative SEM images of small (**c**), middle (**d**), and large-sized (**e**) tetrahedra used for extent of truncation measurement. (**f**,**g**) Distributions of the truncation length L_T and edge length L for differently sized tetrahedral NPs. Scale bars: 100 nm.

2. We performed CD measurements of a suspension of dispersed tetrahedral NPs. As shown in the new Supplementary Fig. 1d, no CD signal was obtained over the wavelength range of 300–800 nm where the assembled pinwheels exhibit chiroptical activity. This result shows that individual tetrahedral NPs do not have a uniform chirality before assembly, even if chirality exists due to the hard-to-visualized effect of uneven distribution of CTAB ligands on the NP surface. This result is also consistent with the lack of chiroptical activity for the corner-sharing honeycomb structures ($\Delta = 0$, Supplementary Fig. 16). Experimentally, to obtain the chiroptically active pinwheel lattice, we used a high concentration of CTAB (1 mM, close to its critical micelle concentration) as the initial concentration as the optimal condition. This high solution concentration of CTAB is expected to prevent net CTAB desorption from the NP surface and ensure the full and uniform surface coverage of CTAB bilayer on the NP surface (*Langmuir* 2012, 28, 1453–1459; *ACS Omega* 2020, 5, 4943–4952).

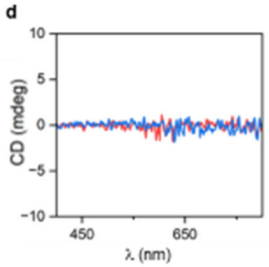

Supplementary Fig. **1d**. CD spectrum of a suspension of dispersed middle (red) and large (blue) sized tetrahedra. The particle optical density (OD) is ~ 1.8 at λ_{max}. These two types of NPs were measured because they could assemble into the chiroptically active pinwheel lattices.

3. Though we do not observe the existence of single NP chirality or the effects of such chirality on the lattice's optical properties, we appreciate the inspirational comment of the reviewer on how single NP chirality translates to superlattice chirality for our strategy in general. We added FDTD simulations (new Supplementary Fig. 17) on a hypothetical system of tetrahedral NPs constructed with chiral extent of truncation much like a lactic acid (Supplementary Fig. 17h where all the corner truncations are different). We systematically arranged them into 4-NP cluster (the smallest chiral motif for the pinwheel lattice), and 72-NP pinwheel lattice, with the NPs arranged either in a random or aligned fashion considering their handedness. As shown in Supplementary Fig. 17, we consistently see no difference in their CD response from the same structure formed from perfectly uniform, achiral tetrahedral NPs.

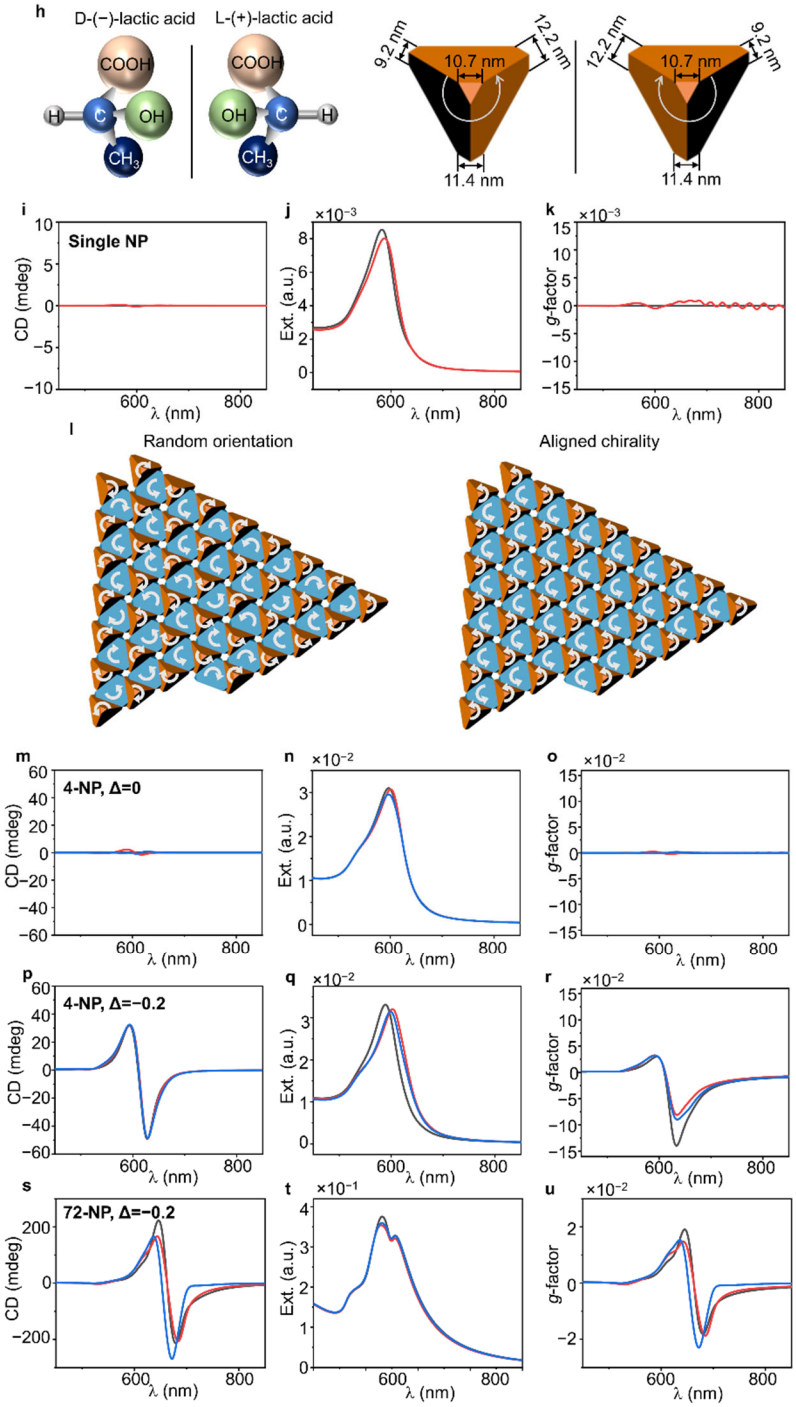

Supplementary Fig. 17h–u. FDTD simulations for corner truncation effect. (**h**) Schematics of the hypothetical chiral tetrahedral NPs and the analogue with enantiomers of lactic acid. (**i–k**) Simulated (**i**) CD spectra, (**j**) extinction spectra, and (**k**) *g*-factor spectra of single NP without (black) and with (red) truncation difference at different corners. (**l**) 72-NP pinwheel lattices used in FDTD simulation, considering the generic chirality on the single NP level induced by corner truncation difference. Arrow direction indicates the orientation from small truncation to large truncation. Simulated (**m,p,s**) CD spectra, (**n,q,t**) extinction spectra, and (**o,r,u**) *g*-factor spectra of 4-NP

cluster of Δ = 0 (**m**–**o**) and Δ = −0.2 (**p**–**r**), and 72-NP pinwheel lattice of Δ = −0.2 (**s**–**u**). Black curves represent the results for tetrahedral NPs without truncation difference at different corners, red curves represent the results for tetrahedral NPs with randomly distributed chirality, and blue curves represent the results for tetrahedral NPs with aligned chirality. We did not see significant differences in the CD response among the structures assembled from NPs with single particle chirality, from the same structure formed from perfectly uniform, achiral tetrahedral NPs. Details of the simulation can be found in Supplementary Note 5.

To address the reviewer's comment, we have included these insights in Supplementary Figs. 1, 2 and 17, "Methods", Supplementary Notes 1, 5, and the main text:

> "We have also verified that the chirality of the pinwheel lattice is not originated from the possible generic chirality of the tetrahedral building blocks due to uneven corner truncations or distributions of surface ligands (Supplementary Figs. 1,2,17, Supplementary Note 5)."

Comment 2: *For a CTAB-based system, it is well known that the bilayer might be disrupted due to desorption of the surfactant molecules during sample preparation, such as drying/washing of the sample. Would this affect the outcome of the assembly process?*

Reply: We thank the reviewer for the great comment. Fundamentally, as we discussed in the manuscript, the bilayer self-assembly is driven by a balance of van der Waals (vdW) attraction between the Au part of the NPs and electrostatic repulsion from the charged ligands.

1. When the charged ligands are CTAB molecules, their packing density on the NP surface is crucial to the assembly. To illustrate this point, in the revised manuscript, we added new experimental data of the assembled structures formed at different initial CTAB concentrations (a new Supplementary Fig. 3). For example, 0.01 mM CTAB is of low enough concentration to cause stripping of CTAB ligands from the NP surface, leading to limited electrostatic repulsion. Face-to-face assembly was observed due to complete collapsing of bilayer lattice (Supplementary Fig. 3f). Meanwhile, at a CTAB concentrations higher than 1 mM to ensure full coverage of CTAB on the NP surface, we do not see structural difference in the assembled bilayer, only with a domain size difference.

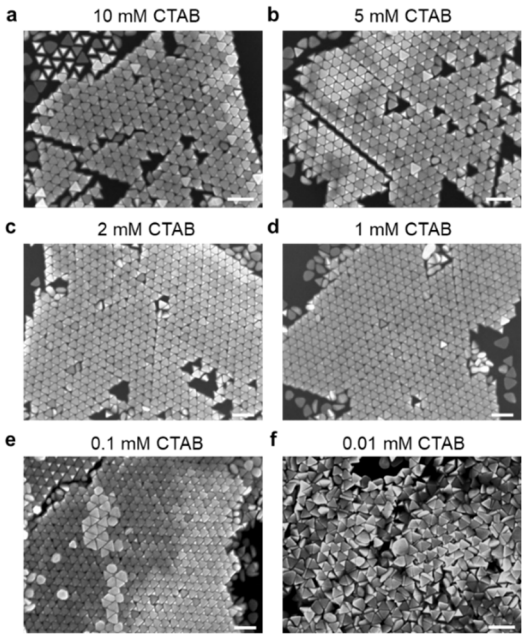

Supplementary Fig. 3a–f. Assemblies of tetrahedral NPs formed with different initial CTAB concentration. SEM images of bilayer assembly of large-sized tetrahedra with initial CTAB concentration of (**a**) 10 mM, (**b**) 5 mM, (**c**) 2 mM, (**d**) 1 mM, (**e**) 0.1 mM, and (**f**) 0.01 mM. Largest bilayer domains were formed at CTAB concentration of 1–2 mM. When the CTAB concentration was 0.01 mM, the dominant assembly structure was face-to-face assembly due to the absence of enough electrostatic repulsion to stabilize the bilayer structure. Scale bars: 200 nm.

2. As to the effect of the CTAB bilayer collapsing upon complete drying of the solvent, we provided discussion on the stability of the bilayer lattice in the original Supplementary Note 3:

   "Theoretical modeling based on these two interactions predicts quantitatively the bilayer structures observed in our experiments (Fig. 4e–g). As discussed previously in the literature, by optimizing the solvent evaporation time to be 6 to 8 h, the assembled structures dictated by solvent-mediated interaction can still be maintained after complete evaporation of the solvent[1,2].

   In the dry state, our measured geometric parameters for *D* (9.7–12.7 nm, see Supplementary Table 3) are larger than two cetyltrimethylammonium bromide (CTAB) bilayers (6.4 nm)[3], suggesting that CTAB bilayers as the ligands on the NPs are not in touch with each other or filling fully the gap between top layer tetrahedra and bottom layer tetrahedra. In this case, the stability of bilayer lattices can be mostly attributed to the fact that our tetrahedral NPs have truncation out of synthesis.

   The truncated corners of the top layer tetrahedra can thus sit on the substrate, stabilizing the top layer NPs even after drying. The resulted attraction between the substrate and the truncated corners will barely allow free sliding of the tetrahedra and thus preventing falling apart of the lattice. We also consistently observed an organic film covering the surface of bilayer assemblies during SEM imaging, which can be resulted from either CTAB or other hydrocarbon species adsorbed during evaporation. The organic film covering the whole surface of lattice may also assist with the stability of the open lattice structure."

3. Lastly, we would like to note that the electrostatic repulsion needed for the bilayer assembly does not necessarily come from CTAB. In our liquid-phase TEM experiment, to ensure NP's stability under electron beam (strategies presented in our earlier work *Nat. Mater.* 2020, 19, 450–455), we used a charged thiol to replace CTAB ligands on the tetrahedral NPs and still observed the bilayer structure (Fig. 4d, Supplementary Fig. 20b).

To address the reviewer's comment, we added the new Supplementary Fig. 3, and added discussion of the result in Supplementary Note 3.

"The charged ligand density on the NPs is crucial to the assembly. Assembly experiment using different initial CTAB concentration (0.01−10 mM, Supplementary Fig. 3a–f) shows that 0.01 mM of CTAB is of low enough concentration to cause stripping of CTAB ligands from the NP surface, leading to limited electrostatic repulsion. Face-to-face assembly was observed instead as a result of complete collapsing of bilayer lattice (Supplementary Fig. 3f)."

Comment 3: *How large can the self-assembled structures be? what is the limit of the vertical thickness?*

Reply: In the revised manuscript, we made the following revisions to address the reviewer's comments:

1. We included more SEM images of the assembled structures (bilayer and multilayers) in the new Supplementary Figs. 8a,b and 24. As shown in Supplementary Fig. 8b, the lateral dimension of a single continuous bilayer domain can be as large as 37 μm^2 and the whole sample area is on the 0.1 mm^2 scale. Our on-going research effort uses a blade assisted evaporation process which can further increase the lateral area of assembled structure by minimizing the coffee ring effect. The vertical thickness of the assemblies depends on the evaporation speed and the ionic strength (see

discussions on Fig. 4f,g), and we have observed the vertical thickness up to five bilayers with well-defined bilayer structures in our experiment (the new Supplementary Fig. 24). Note that to our knowledge, there is no physical limit of the vertical thickness, which can be further extended by increasing NP concentration and the evaporation speed.

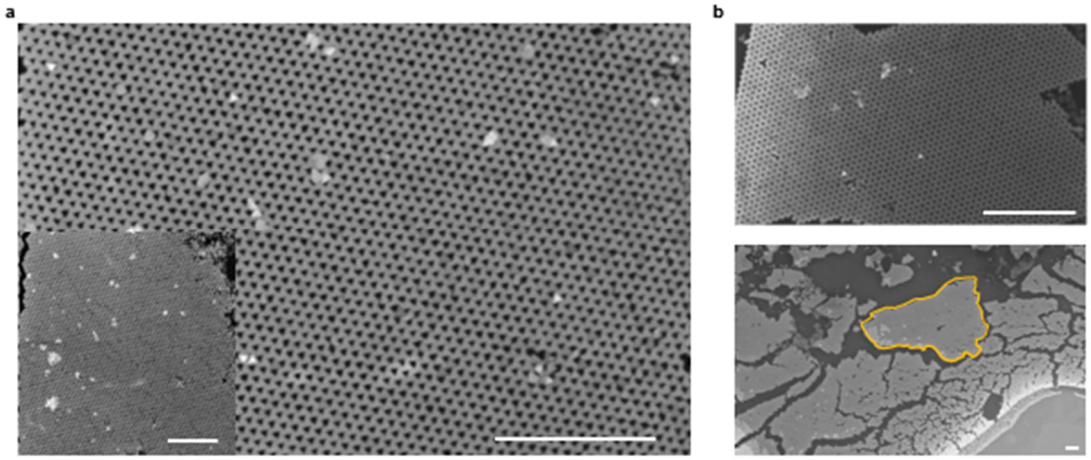

Supplementary Fig. 8a,b. (**a**) SEM images of large-scale bilayer pinwheel lattice (the same sample as that in Fig. 2e) on Si wafer. (**b**) Additional SEM images showing the large-scale bilayer assembly formed at the same condition as (**a**). The domain with yellow contour (bottom) has a lateral dimension of 37 μm^2. Exact assembly conditions can be found in Supplementary Table 2. Scale bars: 1.2 μm (**a,b**).

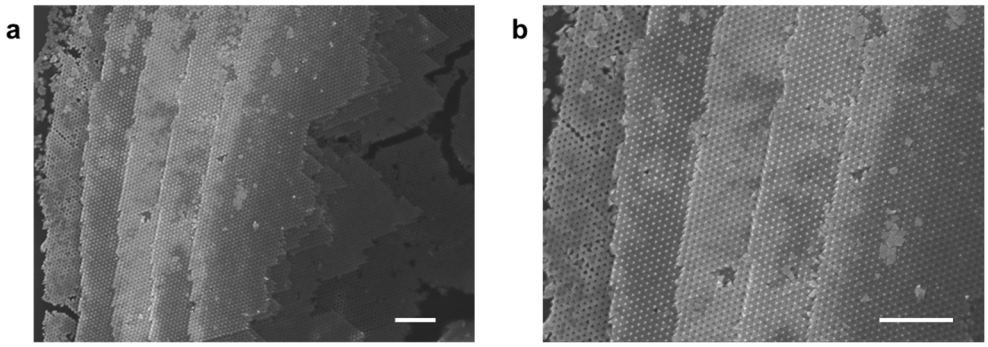

Supplementary Fig. 24. Multilayer assembly formed at a higher initial salt concentration. (**a,b**) SEM images showing multilayer assembly with five bilayers along the vertical direction. Exact assembly conditions can be found in Supplementary Table 2. Scale bars: 1 μm.

2. We have revised discussions in the main text,

"The pinwheel lattices with corner-to-edge connections and thus greater packing fractions are achieved when a spontaneous in-plane compression is induced by weakening E_{el} and/or increasing E_{vdW}. For example, large tetrahedra (L = 68.6 nm) increase E_{vdW}, and hence, form extended domains (>35 μm^2, Supplementary Fig. 8) of pinwheel packing (Fig. 2e) with corner-to-edge contacts, where decreased D and increased packing fraction are observed (Fig. 1c)."

"Multilayer structures (Supplementary Fig. 24) with corner protrusion in all the top bilayers (Fig. 4h) or tilted assemblies without three-fold symmetry (Fig. 4i) are formed, rendering them truly chiral even in the absence of substrate."

Comment 4: *A more quantitative measure of the water evaporation and self-assembly process would be helpful. Right now, it was stated that the evaporation was controlled by pressing the petri dish, which seems to be vague to me.*

Reply: We thank the reviewer for helping us clarify the experimental setup. In the revised manuscript, we have made the following changes.

1. We now added the photo of our assembly setup and how the size of the solution droplet changes over the evaporation process as a new Supplementary Fig. 27. We have measured the evaporation condition inside the setup, which was optimized at 75–80% humidity and 68–71 °F to achieve the controlled evaporation.

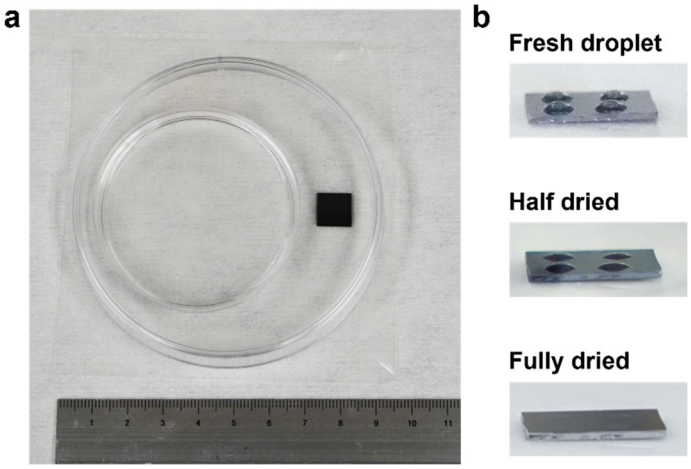

Supplementary Fig. 27. Photos of the assembly setup and the typical drying process we used to obtain the pinwheel lattices. (**a**) The top view of the assembly setup, with Si wafer placed next to the water container covered by a large petri dish to control the humidity of the process. (**b**) Photos of the drying process of four droplets casted on the Si wafer. The optimal evaporation condition has a humidity of 75–80% and temperature at 68–71 °F. The total evaporation time to achieve largest bilayer assembly is 6–8 h.

2. We added corresponding description of Supplementary Fig. 27 in "Methods":

"As shown in Supplementary Fig. 27, a parafilm was cut to the size of 4 inch × 4 inch and placed on top of a TechniCloth (TX 609, Texwipe). The cover of a small petri dish (60 mm × 15 mm, Fisherbrand) filled with water was placed on the parafilm. A small Si wafer (1 cm × 1 cm) was first cleaned with acetone, isopropanol, and water. 2 μL of the thoroughly mixed NP solution was then drop-casted on the Si wafer that was placed next to the small petri dish. Typically, 4–6 droplets were casted on the same wafer for the assembly. Right after dropcasting, the silicon wafer and the petri dish were covered by a large petri dish (100 mm × 15 mm, VWR). The large petri dish was gently pressed to ensure sealing with the parafilm underneath and thus to maintain a humid environment (humidity of 75–80%). A typical optimal drying process takes 6 to 8 h at the temperature of 68–71 °F."

Responses to Reviewer 2

Reviewer 2 enjoyed reading our manuscript and regarded our work as "*very exciting as they can pave the way to unprecedented applications*". We thank the reviewer for the great comments, all of which we have addressed with new experiments (new Supplementary Fig. 8) and calculations (new Supplementary Fig. 17, Supplementary Table 7), particularly on the substrate effect.

Comment 1: *As far as I understand, each nanoparticle cluster has a well-defined sense of handedness while the whole ensemble is racemic, isn't it? Is there a way to push the system to a particular side during the symmetry breaking? Can one potentially try using chiral surfactants or apply an external perturbation such as circularly-polarized light? I would appreciate a short discussion of this point.*

Reply: We thank the reviewer for the insight comment. As the reviewer commented, each NP cluster or domain (> 35 μm^2 as shown in our new Supplementary Fig. 8a,b) has a well-defined handedness, and the ensemble of all the domains on the substrate is expected to be racemic. We agree a discussion on future strategies to direct the handedness to a particular side would be helpful to the community.

In the revised manuscript, we have now added additional references and discussions in the conclusion:

> "Possible strategies to push the handedness of our pinwheel lattice to one side could be using chiral molecules[2] that provide a chiral bias to direct the packing order of NPs via coordination, electrostatic interaction and hydrogen bonding, and circularly-polarized light[35] to adjust the asymmetric displacement of NPs under the asymmetrical electronic and magnetic fields from beam sources, which have proven effective for other gold NPs including gold nanorods and gold nanospheres."

Comment 2: *As pointed by the authors, single-layer structures become chiral due to the presence of the substrate. Did the authors attempt to use different substrate materials to demonstrate the substrate influence experimentally, for example in optical activity?*

Reply: We thank the reviewer for this great comment. We have explored different substrate materials in our work such as silicon, glass slide, and SiN_x, and have now included new data to show their influence on the assembly structures (see the new Supplementary Fig. 8f–h). For each substrate, the bilayer structures are shown to robustly form under proper surface treatment and assembly conditions. This observation is consistent with the assembly mechanism we discussed in Supplementary Note 3: the assembly is driven by a balance of vdW attraction between Au and electrostatic repulsion provided by the charged ligands, while the substrate serves as a support for the tetrahedra NPs to sit on and stand. Regarding optical activity, once the bilayer structure is formed, the presence of SiN_x substrate that was used for the photon-induced near-field electron microscopy (PINEM) measurement is to break the inversion symmetry (Supplementary Figs. 9, 10, and the new Supplementary Fig. 17e–g), and does not significantly impact the chiroptical activity. Note that Si wafer substrate has a large dielectric constant which can induce coupling with the superlattice's optical property. Thus in our work, we consistently used SiN_x substrate for the PINEM measurement to examine the chiroptical responses of the pinwheel lattice.

In the revised manuscript, we have made the following revisions to address the reviewer's comment:

1. We added more SEM images in Supplementary Fig. 8f–h, including the bilayer assemblies on the silicon wafer, glass slides, and SiN_x substrate.

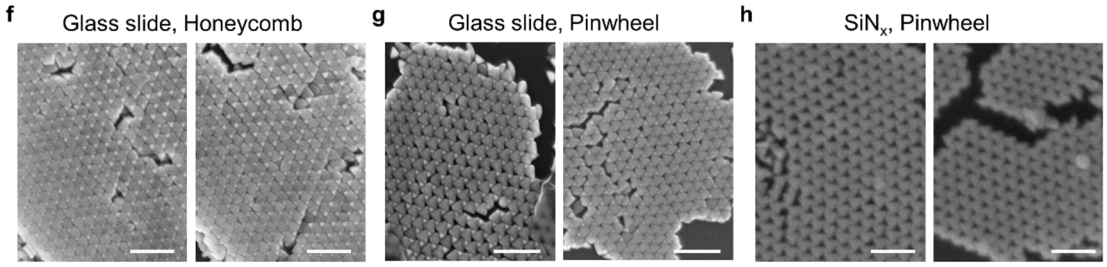

Supplementary Fig. 8f–h. SEM images of bilayers assembled on different substrates: glass slide (**f,g**) and SiN_x membrane (**h**). Exact assembly conditions can be found in Supplementary Table 2. Scale bars: 200 nm (**f–h**).

2. We added discussions on the effect of different substrate materials on the assembled structure in Supplementary Note 3:

"Different substrate materials (including glass slide and SiN_x substrates, Supplementary Fig. 8f–h) have also been used, and similar bilayer structures with tunability can be realized by optimizing the surface treatment and assembly conditions for each substrate material. Fundamentally the assembly is majorly driven by the balance of vdW attraction and electrostatic repulsion between the tetrahedral NPs, and the substrate acts as a support for the assembly and break the inversion symmetry."

We also added discussion on the substrate effect on optical properties in Supplementary Note 5, with new FDTD simulations of the structure (Supplementary Fig. 17e–g) with different substrate materials, including Si (wafer), SiO_2 (glass slide), and SiN_x.

"The experimental PINEM results of the pinwheel lattices on a SiN_x substrate match quantitatively well with the FDTD simulations in Fig. 3c–f where the substrate was not included, suggesting that the substrate–sample interaction does not otherwise influence the chiroptical activity. We further demonstrated that substrate material employed in the PINEM experiments (SiN_x) do not cause major difference in the simulated chiroptical properties of the assembly structures (Supplementary Fig. 17e–g)."

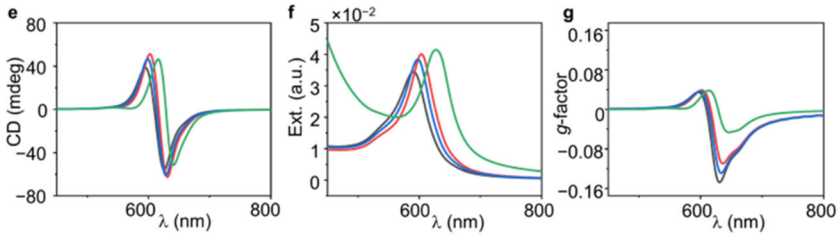

Supplementary Fig. 17e–g. FDTD simulation for 4-NP domain of Δ = −0.2 on different substrates. (**a–c**) CD, extinction, and *g*-factor spectra of 4-NP domain without substrate (black), or placed on Si wafer (green), glass slide (SiO_2, blue) and SiN_x (red). Both SiO_2 and SiN_x have limited impact on the chiroptical responses compared to the result without substrate.

Comment 3: *On line 88 the authors quote the strength of face-to-face nanoparticle repulsion of 0.59 k_BT. Where does this number come from? I did not find it in the supplementary or the main text. By the way, add a space between the number and the "unit" (k_BT).*

Reply: We thank the reviewer for this great comment. We have included more discussions on the strength of interparticle interaction in the revised Supplementary Note 3 and we added Supplementary Table 7 to show the quantitative values, which we now refer to in the main text:

> "The strong face-to-face repulsion (0.59 k_BT, Supplementary Note 3) separates the faces of tetrahedra apart, allowing only corner-to-corner connections, leading to this previously inaccessible low packing fraction lattice."

> "Thus, we find that the sum of one interlayer interaction and two intralayer interactions is able to predict the stable pinwheel structure matching quantitatively the experiments (Supplementary Note 3, Supplementary Figs. 21–23, Supplementary Table 7)."

We also made the format change suggested by the reviewer on k_BT in both main text and Supplementary Note.

Supplementary Table 7. Pairwise interaction calculation results based on coarse-grained model of small tetrahedron using the same experimental geometric parameters as Fig. 4g at 30 mM ionic strength for Δ ranging from 0 to 0.25. $E_{vdW\_1,2}$ and $E_{el\_1,2}$ are van der Waals attraction and electrostatic repulsion between tetrahedra in different layers (T_1 and T_2) respectively. $E_{vdW\_1,3}$ and $E_{el\_1,3}$ are van der Waals attraction and electrostatic repulsion between tetrahedra in the same layer (T_1 and T_3) respectively. Unit: k_BT.

Δ	$E_{vdW\_1,2}$	$E_{el\_1,2}$	$E_{vdW\_1,3}$	$E_{el\_1,3}$	$E_{interlayer}$	$E_{intralayer}$	E_{tot}
0	−1.09	0.59	−0.09	0.02	−0.50	−0.07	−0.63
0.01	−1.12	0.63	−0.09	0.02	−0.49	−0.07	−0.62
0.02	−1.16	0.68	−0.10	0.03	−0.48	−0.07	−0.62
0.03	−1.20	0.73	−0.10	0.03	−0.47	−0.07	−0.60
0.04	−1.24	0.79	−0.11	0.04	−0.45	−0.07	−0.59
0.05	−1.28	0.85	−0.11	0.04	−0.43	−0.07	−0.57
0.06	−1.33	0.92	−0.12	0.05	−0.41	−0.07	−0.55
0.07	−1.37	0.99	−0.12	0.05	−0.39	−0.07	−0.53
0.08	−1.42	1.06	−0.13	0.06	−0.36	−0.07	−0.50
0.09	−1.47	1.14	−0.13	0.06	−0.33	−0.07	−0.47
0.1	−1.52	1.23	−0.14	0.07	−0.29	−0.07	−0.44
0.11	−1.58	1.32	−0.15	0.08	−0.25	−0.07	−0.39
0.12	−1.63	1.42	−0.15	0.08	−0.21	−0.07	−0.35
0.13	−1.69	1.53	−0.16	0.09	−0.16	−0.07	−0.29
0.14	−1.75	1.65	−0.17	0.10	−0.10	−0.07	−0.23
0.15	−1.81	1.77	−0.17	0.11	−0.04	−0.06	−0.16
0.16	−1.87	1.90	−0.18	0.12	0.03	−0.06	−0.09

0.17	−1.94	2.04	−0.18	0.13	0.10	−0.06	−0.01
0.18	−2.01	2.20	−0.19	0.13	0.19	−0.06	0.08
0.19	−2.08	2.36	−0.20	0.14	0.28	−0.06	0.17
0.2	−2.16	2.53	−0.20	0.15	0.38	−0.05	0.27
0.21	−2.23	2.72	−0.21	0.16	0.49	−0.05	0.38
0.22	−2.32	2.92	−0.21	0.16	0.61	−0.05	0.50
0.23	−2.40	3.14	−0.22	0.17	0.74	−0.05	0.63
0.24	−2.49	3.37	−0.22	0.17	0.88	−0.05	0.77
0.25	−2.58	3.61	−0.23	0.17	1.03	−0.06	0.92

Comment 4: *On line 92 the authors use two times the van der Waals energy symbol with the subscript "vdW" and "vdw". Use consistent notations. Line 60 "experimentally realization" -> experimental realization?*

Reply: Thank you! We have now unified the usage of "vdW" in the revised manuscript and changed the language to "experimental realisation" on Line 60.

Responses to Reviewer 3

Reviewer 3 supported our paper for publication in *Nature*, and commented that we "*achieved a previously unknown structure*" which "*break structural symmetries, thereby leading to the unique chiral optical response*". The reviewer considered our work "*presents an innovative experimental demonstration of compelling chiral optical properties arising from unique nanoarchitectures, which is important to the fields of nano-assemblies, optoelectronics, spintronics, and metamaterials*." We also thank the reviewer for the detailed comments, all of which we have now addressed with new experiments (Supplementary Figs. 1e–j, 2c–e, 3g–l, 8a,b), new analysis and pairwise interaction calculation (Supplementary Figs. 2f,g, 21, 22), new schematics and video (Supplementary Fig. 7, Supplementary Video 2), and new FDTD simulations (Supplementary Fig. 25), particularly on experimental verification of surface ligands, additional images of large-scale characterization of tetrahedral NPs and assemblies, and identifying the substrate effect.

Comment 1: *Through reading the paper, I do not quite feel that using the terms of "perovskite" are necessary or even accurate. Normally, perovskite structure retains its octahedral corner connection point during deformation or transformation, which is clearly not the case in this paper. As much as I value this paper, it may not be appropriate to use a buzzword like "perovskite" to show its significance.*

Reply: We thank the reviewer for the comment. In the original manuscript, we used "perovskite" as a reader-friendly analogy to highlight the corner-sharing feature of NP honeycomb lattice and the transition it allows, both of which are novel for NP assemblies. We agree with the reviewer that atomic perovskites keep their corner connections during deformation, while in our system, tetrahedral NPs switch to corner-to-edge connections instead.

In the revised manuscript, we clarified the statement and articulated the difference between the honeycomb lattice and atomic perovskites:

> "Although the inspiration is from atomic systems, the linkages of corner-sharing structures are not permeant chemical bonds but physical colloidal interactions, which allow for different compression pathways and potentially rich design space."
>
> And
>
> "During twisting, corner-to-corner connections originated from physical interactions switch seamlessly to corner-to-edge connections, instead of the corner-to-corner chemical bonds constrained in atomic crystals."

Comment 2: *As I see in Figure 2b-d, it is unclear whether the structure hold the corner-to-corner or face-to-face connection between the neighboring building blocks. It is confusing to me how do the authors define the corner-to-corner or the corner-to-edge superlattices? Is this defined based on the distance? For the corner-to-corner lattice (honeycomb structure), is the distance between two connected corners significantly smaller than that between the two registered faces? How about the corner-to-edge structure?*

Reply: We thank the reviewer for helping us clarify the structures assembled. In Fig. 2b and Fig. 2d, the structures are corner-to-corner, which we also referred to the honeycomb lattices as noted in the original manuscript: "Fast Fourier transform (FFT) of the scanning electron microscopy (SEM) image shows a pattern resembling a honeycomb structure (Fig. 2d)". Quantitatively, we identify the corner-to-corner (i.e., honeycomb) lattice when we observe a corner offset Δ close to 0 (see the definition we now included in Supplementary Note 1, experimentally $\Delta \leq 0.05$); and the corner-to-edge (i.e., chiroptically active pinwheel) lattice when Δ is deviated from 0 (experimentally $\Delta > 0.05$). Note that Δ is also the quantitative measure to predict if the structure is chiroptically active or not.

For the honeycomb structure, the corner-to-corner distance (defined as D_{c-c}) is indeed smaller than the distance between two registered faces (D). For the corner-to-edge pinwheel structure, however, D_{c-c} can be sometimes larger than D given a structure with high Δ.

To comprehensively address the reviewer's comment, we have made the following changes in the revised manuscript,

1. We have now added the definition of corner-to-corner distance D_{c-c} in Supplementary Note 1, the experimental values of the corner-to-corner distance D_{c-c}, distance between two faces D, and corner-to-edge distance L_{e-c} for all the assembled structures presented in Fig. 2 and Fig. 4 in the revised Supplementary Table 3.

   Supplementary Table 3. Geometric parameters for bilayer lattices shown in Fig. 2 and Fig. 4.

Sample ID	L_P (nm)	L_{e-c} (nm)	D_{f-c} (nm)	D (nm)	D_{c-c} (nm)
Fig. 2d	47.2 ± 1.6	8.2	7.7	11.0	8.5
Fig. 2e	89.4 ± 1.8	17.4	16.4	9.2	50.9
Fig. 4d	104.9 ± 6.9	19.0	18.0	25.9	22.0
Fig. 4g−star	47.5 ± 2.6	8.1	7.7	11.2	8.7
Fig. 4g−circle	61.2 ± 3.8	9.6	9.0	11.4	11.1
Fig. 4g−diamond	86.9 ± 5.5	14.0	13.2	12.7	33.1
Fig. 4g−square	89.1 ± 6.3	16.5	15.5	9.7	47.2

2. We added clarification in the main text,

   "Variation of NP size, ionic strength and molecular additives results in systematic changes of $|\Delta|$ from 0.03 to 0.56 (Supplementary Figs. 5,6, Supplementary Table 4). In the experiment, we differentiate the corner-sharing honeycomb lattice and corner-to-edge pinwheel lattice using a threshold Δ of 0.05 (Supplementary Table 4)."

Comment 3: *Authors claimed that the tetrahedral gold nanocrystals used in this study are coated with both CTAB (on the faces) and thiol (on the corners), but I do not find the synthetic details about how the authors achieve this asymmetric ligand coverage. Authors should also provide direct evidence to show there are indeed two types of ligands on the particle surfaces. In addition, it is known that the ligand coating on the shaped metal nanocrystals is not uniform (less dense on the corners than on the face), which may play roles when considering the interparticle interactions. Do authors consider this effect? For example, if there is no thiol ligand coverage on the corner, is the structure trapped in the corner-sharing honeycomb structure?*

Reply: We thank the reviewer for the great comment. While it is experimentally challenging to directly map the spatial distribution of ligands on a NP surface (this itself will be a breakthrough in nanoparticle science, such as the recent work: *Nano Lett.* 2019, 19, 6308–6314), we have the conclusion that both CTAB and thiol are present on the surfaces of the tetrahedral NPs using other characterizations. CTAB has been regarded as the stabilizing ligand in the gold NP synthesis on {111} facets (the facets for both the truncation sites and the four major faces of tetrahedral NP; see details in *Chem. Asian J.* 2014, 9, 2635–2640). The

zeta potential of tetrahedral NPs before thiol incubation is +56.6 ± 10.9 mV and that of tetrahedral NPs after thiol incubation is +53.0 ± 8.84 mV, which suggests no significant surface charge change after introducing thiol and the dominance of CTAB ligands on the NP surface. Meanwhile, we found that introducing thiol molecules can prevent the corner truncations of the tetrahedral NPs after 11 days (see the new SEM images provided in Supplementary Fig. 3k,l), from which we infer that thiol molecules are likely adsorb on to the corners and assist the preservation of NP shape. In the literature of ligand exchange, it has also been shown that thiol molecules (when used at a low concentration such as 0.023 mM/particle OD at λ_{max} in our experiment) would preferentially adsorb onto the corners of polyhedral NPs (see our previous work: *J. Am. Chem. Soc.* 2019, 141, 11796–11800 where thiol preferentially adsorb onto the corners of polyhedral at 0.12 mM/particle OD at λ_{max}; and demonstrated by others in experiments and simulations: *J. Am. Chem. Soc.* 2003, 125, 13914–13915; *Nanoscale*, 2012, 4, 2640–2650; *J. Am. Chem. Soc.* 2017, 139, 9851–9854; *ACS Sustainable Chem. Eng.* 2022, 10, 7330–7340).

It is a good point that the corners might adopt different ligand density compared to the facets. In our case, truncated tetrahedra have {111} facets at both the truncation sites and its four major faces, so we regard them to be the same with the same charged ligand density in our pairwise interaction calculations, which are consistent with our experimental observation. We now show below even if considering a lower charge density of the corner than that of the major facet, the interaction calculation still favors the same bilayer structure.

In the revised manuscript, we have made the following changes to address the reviewer's comment:

1. We added a new Supplementary Fig. 3g–l showing that without thiol coverage on the NP corner, tetrahedral NPs can still form into the same library of structures we observed in the presence of thiol coverage (e.g., honeycomb, pinwheel, face-to-face assembly) at different conditions instead of getting trapped in the corner-sharing honeycomb structure. The difference is that without thiols, the assemblies or NPs can have their corner rounded over time.

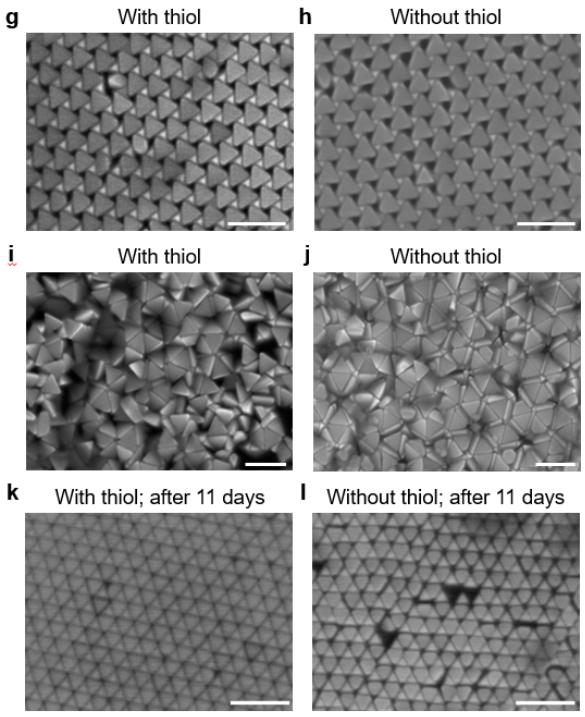

Supplementary Fig. 3g–l. Assemblies of tetrahedral NPs formed at different initial thiol concentration. (**g–j**) SEM images of large-sized tetrahedra with (**g,i**) and without (**h,j**) thiol that

form into pinwheel and face-to-face assembly. The images were taken right after the samples were prepared. (**k,l**) SEM images of bilayer assembly of middle-sized tetrahedra with (**k**) and without (**l**) thiol after 11 days. Tetrahedral NPs turning rounded without the stabilization by thiol. Exact assembly conditions can be found in Supplementary Table 2. Scale bars: 200 nm.

2. We added a new Supplementary Fig. 21 to include new pairwise interaction calculations showing that even considering less CTAB coverage at the corners, the bilayer structure is still stable (Supplementary Fig. 21). We added details and discussions on this calculation in Supplementary Note 3.

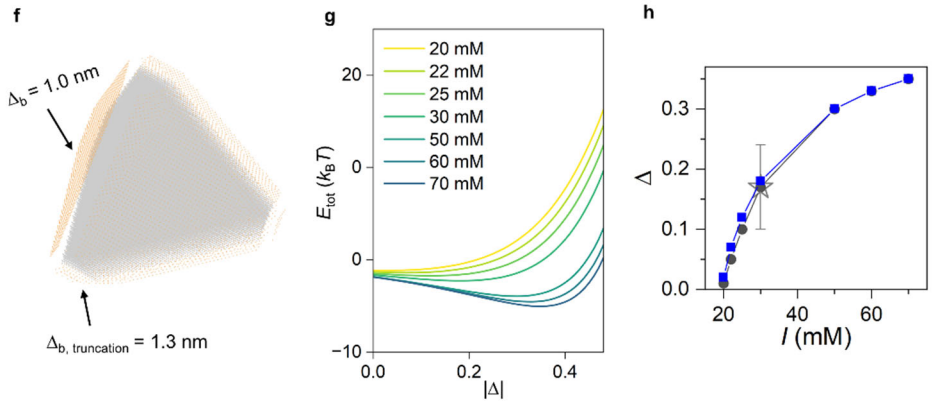

Supplementary Fig. 21f–h. Interaction calculations of tetrahedral NPs assembled into bilayer lattices using coarse-grained model. (**f**) Snapshot from calculation showing the model for different charged ligand density at corners. (**g**) Interaction calculation of tetrahedral bilayer with different charged ligand density for middle-sized tetrahedra at different ionic strengths. (**h**) Comparison of optimal |Δ| between with (blue line with filled square markers) and without (black line with filled circle markers) different ligand density at face and truncation. Unfilled star marker with error bar represents the experimental Δ and its standard deviation. Comparing to tetrahedra with no charge difference at corners, the interaction calculations for middle-sized tetrahedra with a lower charge density at corners show no significant differences in stability and Δ. All geometric parameters including L, L_T, and $L_{e\text{-}c}$ are based on experimental results (Supplementary Tables 1,3).

3. We added new discussions on bilayer structure is still preferred even if considering a lower charge density on the corners in the Supplementary Note 3.

Comment 4: *When the pinwheel structure is formed and evolved, do the faces of neighboring tetrahedra remain parallel? How about the registration area change between the two touching faces during the process? I would imagine the area should be getting smaller during the "compression" process, which in turn alters the interparticle interactions (for both electrostatic repulsion and van der Waals attraction). Can the authors comment on it?*

Reply: We thank the reviewer for the great questions.

1. During the transformation, the faces of neighboring tetrahedra have to remain parallel due to the equilateral constraint and energy constraint. In the revised manuscript, to illustrate this point quantitatively, we have now included new interaction calculations (see the new Supplementary Fig. 22) showing that adopting parallel configurations is more thermodynamically stable than adopting unparallel configuration.

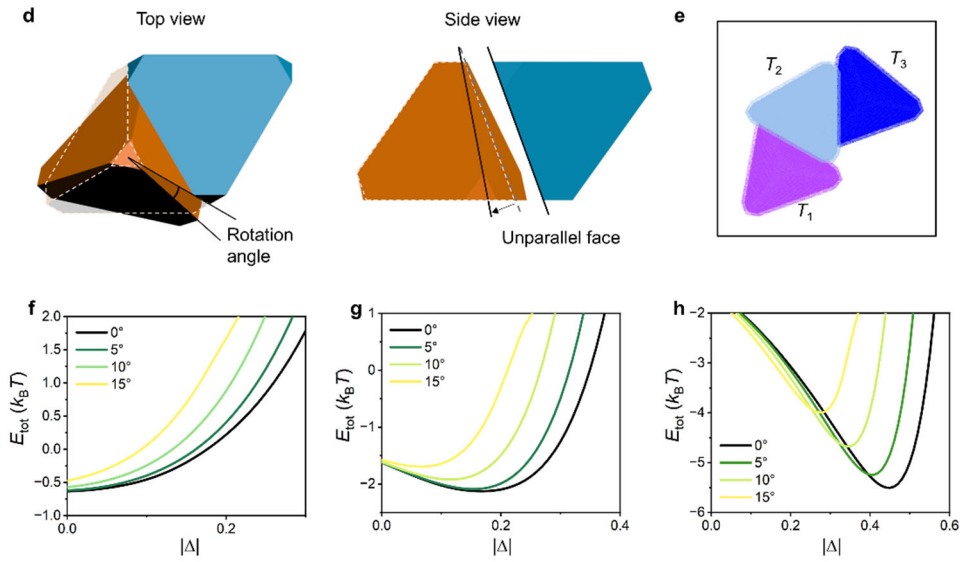

Supplementary Fig. 22d–h. Interaction calculation of tetrahedral NPs assembled into bilayer lattice with unparallel faces. (**d**) Schematics showing an unparallel pair of tetrahedra after rotation in top view and side view. (**e**) Snapshot from interaction calculation showing T_1 and T_3 rotate clockwise with a rotation angle = 10˚ without changing their positions at a certain Δ. (**f–h**) Interaction calculations of the three-tetrahedra model for small (**f**), middle (**g**) and large-sized (**h**) tetrahedra at different rotation angles at I = 30 mM. All geometric parameters including L, L_T, and $L_{e\text{-}c}$ are based on experimental results (Supplementary Tables 1,3).

2. Indeed the registration area (or the overlapped area) between the two facets of the neighboring tetrahedra becomes smaller during the "compression" process. In the revised manuscript, we now included the schematics of this registration area change in the new Supplementary Fig. 7a–c to show its dependency on the corner offset Δ or the effective extent of "compression".

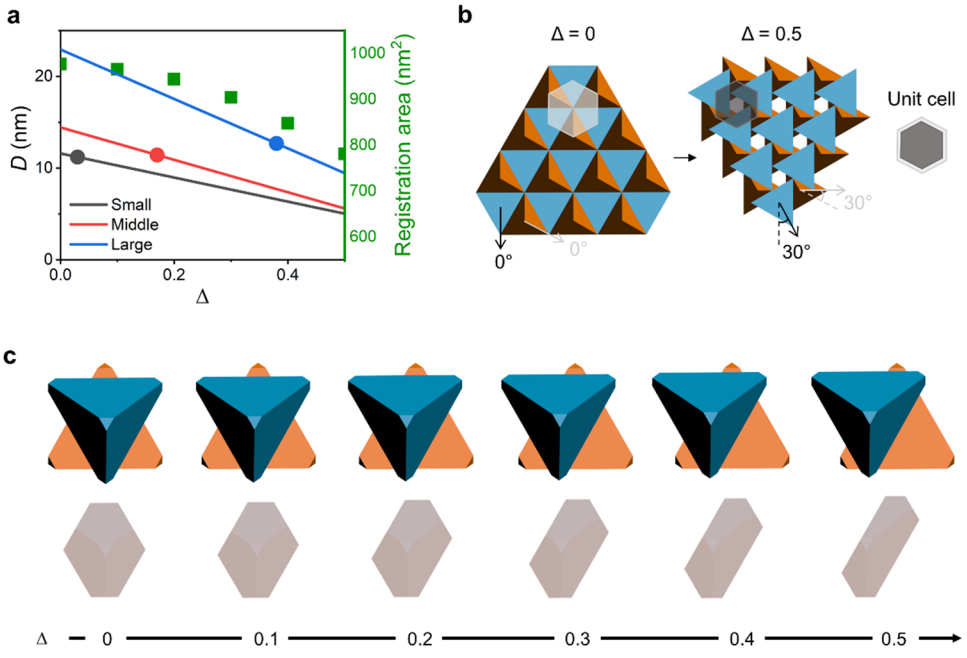

Supplementary Fig. 7. Geometric parameter and schematics of the structural change of the bilayer lattice as a function of Δ. (**a**) Relationship between D and Δ for small, middle, and large-sized tetrahedron bilayer self-assemblies, and relationship between registration area and Δ for middle-sized tetrahedron bilayer lattices. D here are calculated by using parameters measured under experiment conditions considering $L_{e\text{-}c}$: $D = \frac{\left|L-\sqrt{2}L_T+\left(\frac{\sqrt{3}}{3}+\sqrt{6}\right)L_{e-c}-\sqrt{2}|\Delta|\left(L+L_T+\frac{2\sqrt{3}}{3}L_{e-c}\right)\right|}{3\sqrt{3}}$. All parameters used for calculation are summarized in Supplementary Tables 1,3. The circular markers indicate D calculated using the experimental Δ from Fig. 4g-star, Fig. 4g-circle and Fig. 4g-diamond (Supplementary Table 4). (**b**) Schematics showing the transformation from achiral honeycomb lattice to chiral pinwheel lattice after individual NP rotates 30° (Δ = 0.5). The packing fraction of the bilayer is inversely proportional to the volume of the unit cell, and the ratio of the unit cell volume change before and after rotating 30° is $\frac{V_{\text{unit cell, }\Delta=0.5}}{V_{\text{unit cell, }\Delta=0}}=\frac{3}{4}=\frac{\frac{1}{P_{F,\Delta=0.5}}}{\frac{1}{P_{F,\Delta=0}}}=\frac{\frac{1}{3}}{\frac{4}{9}}$. (**c**) The Schematics showing the registration area between two neighboring tetrahedra faces as a function of Δ.

Comment 5: *I would like to see more detailed characterizations of the tetrahedral gold nanocrystals (after depletion purification) used for assemblies. TEM and SEM images for large area survey and individual particles with statistical analyses of the particle geometry should be provided. I do not question the size and shape determined by the authors, but I would appreciate if the authors could provide these raw data to the readers.*

Reply: We thank the reviewer for the suggestion! In the revised manuscript, we now included a lot more (**29** new images in total) TEM and SEM images of large area survey and individual NP analysis with statistics (Supplementary Figs. 1 and 2), the robustness of the bilayer structures (including honeycomb and pinwheel ones) at different conditions (CTAB concentrations, substrate materials, with or without thiols, etc.; Supplementary Figs. 2, 3, 8 and 24—summarized in this reply as Fig. R1) to address comprehensively the reviewer's question.

1. We added more TEM images of the tetrahedral NPs after depletion purification and provided the statistical analysis of the NP geometry with more SEM images provided in Supplementary Figs. 1 and 2.

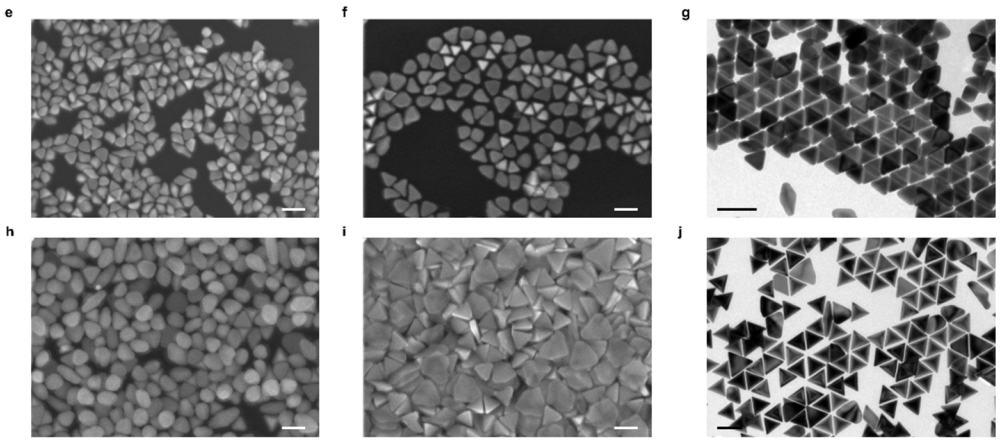

Supplementary Fig. 1e–j. SEM images of impurities (**e,f,h,i**) from the purification of tetrahedral NPs and the TEM images (**g,j**) of tetrahedra after purification. Spherical impurities (**e**) and platelike impurities (**f**) from the purification of middle-sized tetrahedra (**g**). Spherical impurities (**g**) and platelike impurities (**h**) from the purification of large-sized tetrahedra (**j**). Scale bars: 100 nm.

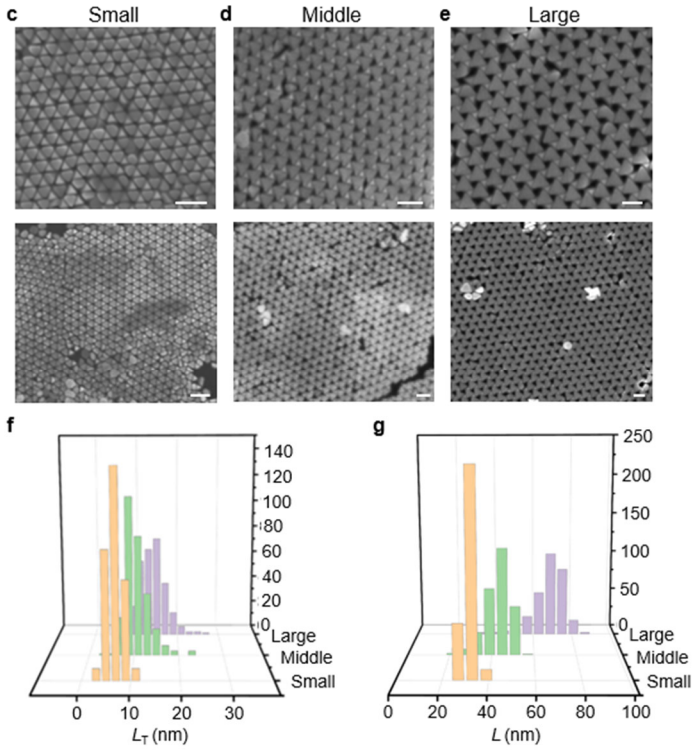

Supplementary Fig. 2c–g. (**c**–**e**) SEM images of small (**c**), middle (**d**), and large-sized (**e**) tetrahedra used for statistics. (**f,g**) Distributions of the truncation length L_T and edge length L for different sized tetrahedral NPs. Details can be found in Supplementary Notes 1 and 2. Scale bars: 100 nm.

2. We added overall more SEM images (21 new images in total, Fig. R1) of the assembled structures which are robustly assembled under different conditions (CTAB concentrations, with or without thiols, Supplementary Figs 3; substrate effect, Supplementary Fig. 8; additional SEM images for multilayer assemblies, Supplementary Fig. 24).

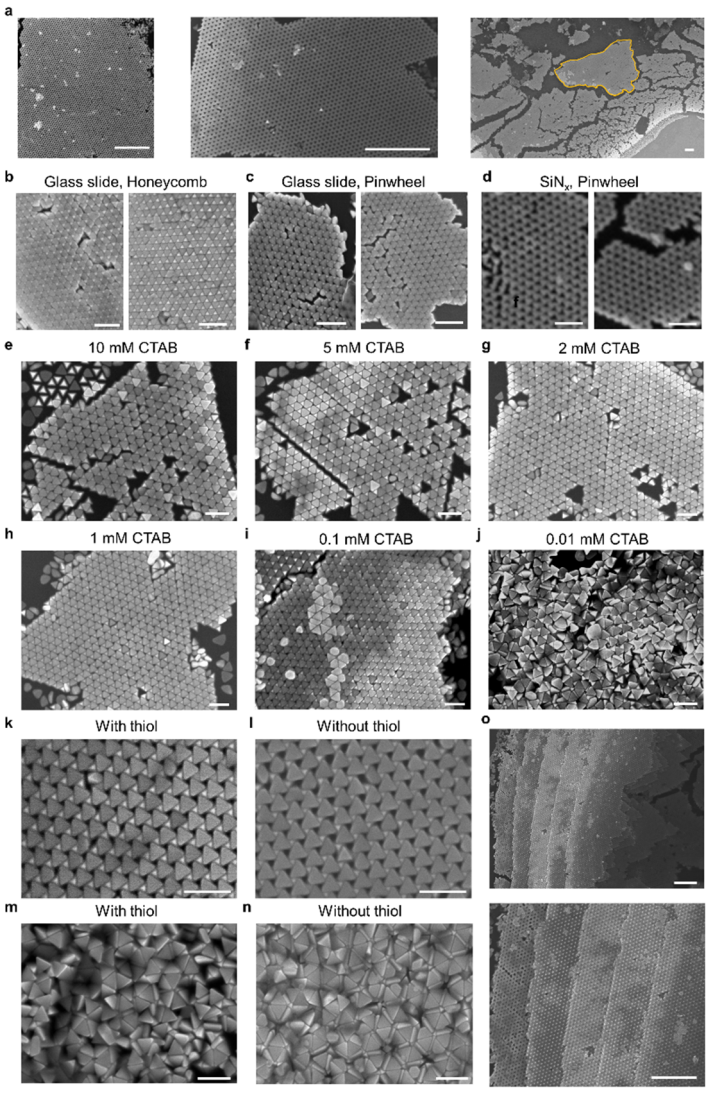

Fig. R1. Additional SEM images showing the rich assembled structures that are robustly assembled under different conditions. (**a**) SEM images of large-scale bilayer pinwheel lattice on Si wafer (Supplementary Fig. 8a,b). (**b–d**) SEM images of bilayers assembled on different substrates: glass slide (**e,f**) and SiN_x membrane (**g**) (Supplementary Fig. 8f–h). (**e–j**) Assemblies of tetrahedral NPs formed with different initial CTAB concentration (Supplementary Fig. 3a–f). (**k–n**) SEM images of assemblies formed at different initial thiol concentration (Supplementary Fig. 3g–l). (**o**) SEM images of multilayer assembly formed at a higher initial salt concentration (Supplementary Fig. 24). Scale bars: 100 nm (**a–c**), 1.2 μm (**d**), 200 nm (**e–q**), 1 μm (**r**).

Comment 6: *The authors mentioned the importance of the domain size to the materials' chiral properties, I am curious about the maximum domain size of the pinwheel superlattices that the authors obtained using this method?*

Reply: We included more SEM images of the assembled structures in the new Supplementary Figs. 8a,b. As shown in Supplementary Fig. 8b, the lateral dimension of a single continuous bilayer domain can be as large as 37 μm^2 and the whole sample area is on the 0.1 mm^2 scale. Our on-going research effort uses a

blade assisted evaporation process which can further increase the lateral area of assembled structure by minimizing the coffee ring effect.

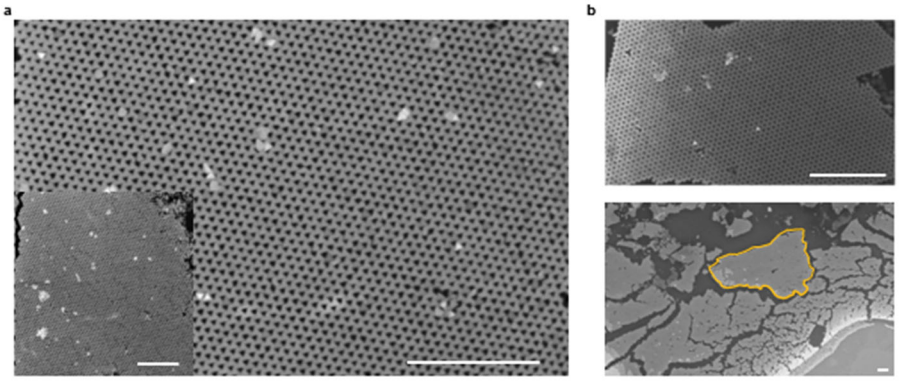

Supplementary Fig. 8a,b. (**a**) SEM images of large-scale bilayer pinwheel lattice (the same sample as that in Fig. 2e) on Si wafer. (**b)** Additional SEM images showing the large-scale bilayer assembly formed at the same condition as (**a**). The domain with yellow contour (bottom) has a lateral dimension of 37 μm^2. Exact assembly conditions can be found in Supplementary Table 2. Scale bars: 1.2 μm (**a,b**).

In the revised manuscript, we have added additional discussions in the main text,

> "The pinwheel lattices with corner-to-edge connections and thus greater packing fractions are achieved when a spontaneous in-plane compression is induced by weakening E_{el} and/or increasing E_{vdW}. For example, large tetrahedra (L = 68.6 nm) increase E_{vdW}, and hence, form extended domains (>35 μm^2, Supplementary Fig. 8) of pinwheel packing (Fig. 2e) with corner-to-edge contacts, where decreased D and increased packing fraction are observed (Fig. 1c)."

Comment 7: *According to the description at the line 101-102, "the effective "compression" increases the packing fraction to 2/3 when all tetrahedra rotate in-plane by 30°." More clarification of this sentence is needed. Having seen chiral assemblies like Figure 3c, or Figure 2e, I find it is difficult to believe that the chiral structure (looks like a more opened structure) is actually compressed and has a doubled packing density as compared to the original honeycomb structure.*

Reply: We thank the reviewer for catching this great point. In the revised manuscript,

1. We now included in the new Supplementary Fig. 7b both the schematics of the bilayer assembly before and after 30° rotation and of how the packing fraction is calculated (Supplementary Fig. 7b).

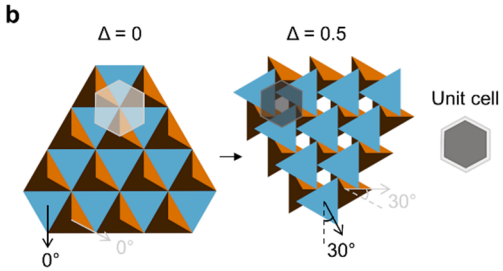

Supplementary Fig. 7b. Schematics showing the transformation from achiral honeycomb lattice to chiral pinwheel lattice after individual NP rotates 30° (Δ = 0.5). The packing fraction of the

bilayer is inversely proportional to the volume of the unit cell, and the ratio of the unit cell volume change before and after rotating 30° is $\frac{V_{\text{unit cell, }\Delta=0.5}}{V_{\text{unit cell, }\Delta=0}} = \frac{3}{4} = \frac{\frac{1}{P_{\text{F},\Delta=0.5}}}{\frac{1}{P_{\text{F},\Delta=0}}} = \frac{\frac{1}{3}}{\frac{4}{9}}$

2. We added new schematics (Supplementary Fig. 7f) to show the volume change of the void regions of the superlattice to highlight that the pinwheel lattice is compressed and has a higher packing fraction than the original honeycomb structure.

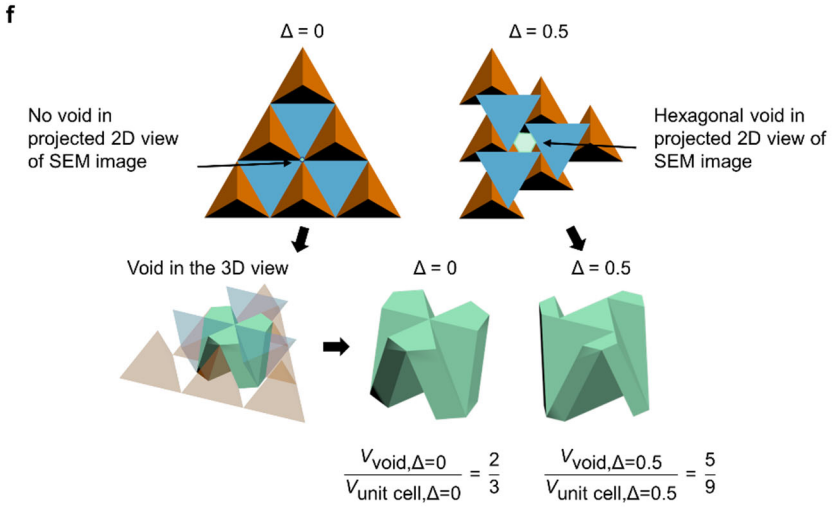

Supplementary Fig. 7f. Schematics showing the volume change of the void regions of the superlattice in 3D, and the projected view of the void in 2D (similar to the direct observations in the top view SEM images, Fig. 2d,e) to highlight that the pinwheel lattice is compressed and has a higher packing fraction than the original honeycomb structure.

3. We revised the discussion in the main text:

"The effective "compression" increases the packing fraction to 4/9 when all tetrahedra rotate in-plane by 30° (Fig. 1b,c, Supplementary Note 1, Supplementary Fig. 7) and changes the point group from D_{3d} to S_6 (Fig. 2c, Supplementary Video 1)."

We apologize for the typographical error of the value of the packing fraction!

Comment 8: *The origin of the chirality, as described in lines 104-108, does not quite make sense to me. Do you know other examples of chirality arising only when the structure is deposited on a substrate (if so, the works should be cited). It would be helpful if the authors can provide some schematic drawings to show this. Is this because of the fixed structure orientation (viewing direction) after sitting on a substrate or different assembly behavior when substrate is presence? Also, in line 107, I do not understand what do the authors mean by "flipping results into an inequivalent mirror image". What is this "inequivalent mirror image?" More explanation and experimental results are needed.*

Reply: We thank the reviewer for the great comment to help us clarify the origin of chirality in this work. Below we detail the changes we have made, including discussions and citations of previous literatures on substrate-induced chirality, schematic drawings of how substrate introduces a symmetry-breaking effect, and more discussions on "inequivalent mirror image", and more FDTD calculations to show how the symmetry-breaking effect presented in the system of tetrahedral NPs can be extended to lattices assembled from other NP shapes.

1. As a summary, there are two components contributing to the chiroptical activity of a superlattice: (i) the lack of in-plane mirror symmetry—the structure cannot overlap with its counterpart created by a mirror perpendicular to the superlattice plane through in-plane rotation; (ii) broken inversion symmetry—the structure cannot overlap with its counterpart through flipping. Our pinwheel lattice satisfies (i) but honeycomb lattice does not; the latter does not exhibit chiroptical activity (Supplementary Fig. 16). Pinwheel lattice does not generically satisfy (ii) as demonstrated in OPD analysis, but the substrate and the pinwheel lattice together as a whole satisfies (ii), which we discussed in the original manuscript, "This effect can be demonstrated by calculating the chirality measure with the Osipov-Pickup-Dunmur parameter[35,36] (OPD) of a freestanding pinwheel lattice in the absence of a substrate (OPD = 0) (Supplementary Fig. 9, Supplementary Note 4, Supplementary Table 5), which becomes either positive or negative indicating the assembly of left and right chirality with inclusion of a substrate (Fig. 3a, Supplementary Fig. 10, Supplementary Table 6)."

   We elaborated these two requirements in Supplementary Note 5.

2. We added previous literatures in the main text discussing a similar mechanism of how substrate can break the symmetry of the deposited structure including top-down fabricated quasi-planar nanostructures (e.g., *Phys. Rev. Lett.* 2005, 95, 227401) and limited-sized nanoparticle assemblies (*ACS Photonics* 2019, 6, 1876–1881). See the details presented in Fig. R2 (Fig. 1 from *ACS Photonics* 2019, 6, 1876–1881). Our work is the first demonstration of this principle to large-scale self-assembled superlattices.

   "We note that free-standing pinwheel superlattices of the corner-to-edge assemblies of tetrahedra are inversion symmetric, but they become chiral when deposited on a flat substrate, similar to early reports on top-down fabricated quasi-planar nanostructures and limited-sized NP assemblies[33,34]."

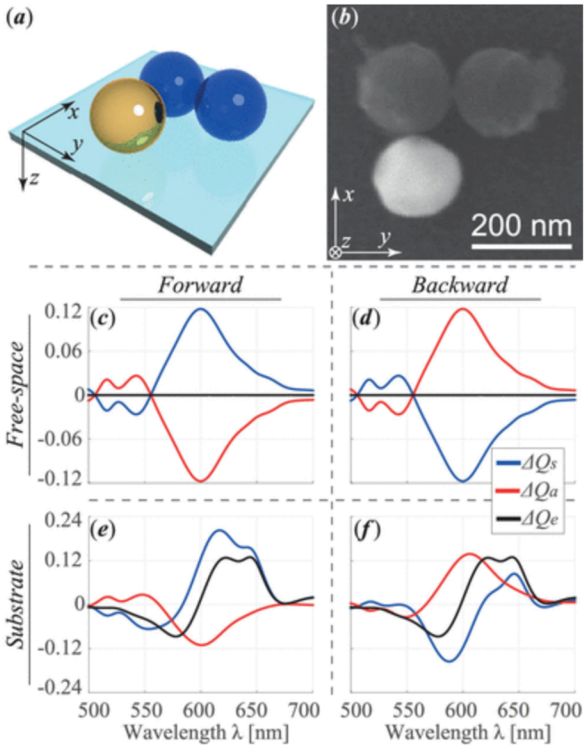

Fig. R2. Substrate-induced chirality in nanosphere assembly. (**a**) Schematics and (**b**) SEM image of the nanotrimer composed of three nanospheres with radii r = 90 nm, arranged in 90° bent

geometry and positioned on a glass substrate. The two upper nanoparticles in (**b**) are made of Si, while the third one is made of Au. (**c–f**) Analytical cross sections, derived from a coupled dipole model of the nanosphere system. (**c**) Normalized differential scattering (ΔQ_s), absorption (ΔQ_a) and extinction (ΔQ_e) cross sections for the nanotrimer in free-space, illuminated with left- and right-hand circularly polarized plane-waves along the positive direction of the z axis ($+\hat{\mathbf{z}}$). (**e**) Same as (**c**) for the nanotrimer on a glass substrate with a refractive index of $n = 1.52$. (**d, f**) Same as (**c**) and (**e**), respectively, for illumination from the opposite direction of the z axis ($-\hat{\mathbf{z}}$). The differential extinction (i.e., CD) cross section of the nanotrimer changes from a constant zero value to non-zero values when it is placed on a glass substrate instead of in the free-space. (Fig. 1 of *ACS Photonics* 2019, 6, 1876–1881).

3. We added additional schematics in Supplementary Fig. 7d,e and Supplementary Video 2 to show how substrate induces chirality:

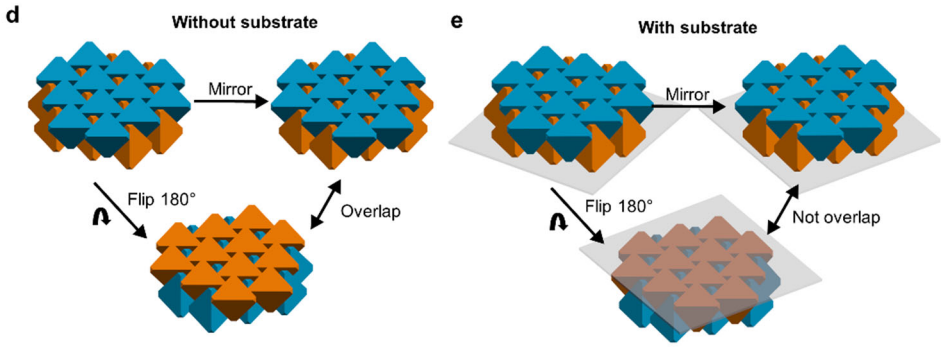

Supplementary Fig. 7d,e. Schematics showing symmetry breaking of the bilayer lattice induced by substrate. Without substrate (**d**), bilayer lattice can overlap with its mirror image through flipping. With the presence of the substrate (**e**), bilayer lattice cannot overlap with its mirror image even after flipping.

We added additional discussions in the main text,

"The pinwheels can be superimposed onto their mirror image if flipping in z direction is allowed, but when the substrate is present, flipping of the structure will lead to the position change of the substrate that leads into an inequivalent mirror image of the original structure (Supplementary Fig. 7, Supplementary Video 2)."

4. We also would like to thank the reviewer for capturing the essence of the substrate effect. As we discussed in our response to Comment 2 of Reviewer 2 and as the reviewer correctly commented, chirality emerges due to the fixed orientation of the structure (or viewing direction) as it sits on a substrate. In terms of the assembled structure, fundamentally the assembly is driven by a balance of vdW attraction between Au and electrostatic repulsion provided by the charged ligands, while the substrate serves as a support for the tetrahedra NPs to sit on and stand (see detailed discussions in Supplementary Note 3).

   As a result, if there is a different factor that could fix the structure orientation, the chirality will emerge too. For example, we did not include explicitly a substrate in our FDTD simulations, but we fixed the structure orientation relative to the direction of the incident light. Therefore inversion symmetry was not allowed and the chirality quantitatively matches with our experimental PINEM maps.

5. We included additional FDTD simulations and show that other types of assembly structures can also demonstrate chiroptical properties, when they lack both the mirror symmetry and the inversion

symmetry (see the two requirements we discussed in bullet point 1). We demonstrated that, for example, the twisted superlattices from nanocubes, which meet these two symmetry-breaking requirements, exhibit CD signal (new Supplementary Fig. 25). In comparison, the hexagonal lattice of nanospheres and square lattice of nanocubes do not lack mirror symmetry and thus do not exhibit CD signal even in the presence of a substrate.

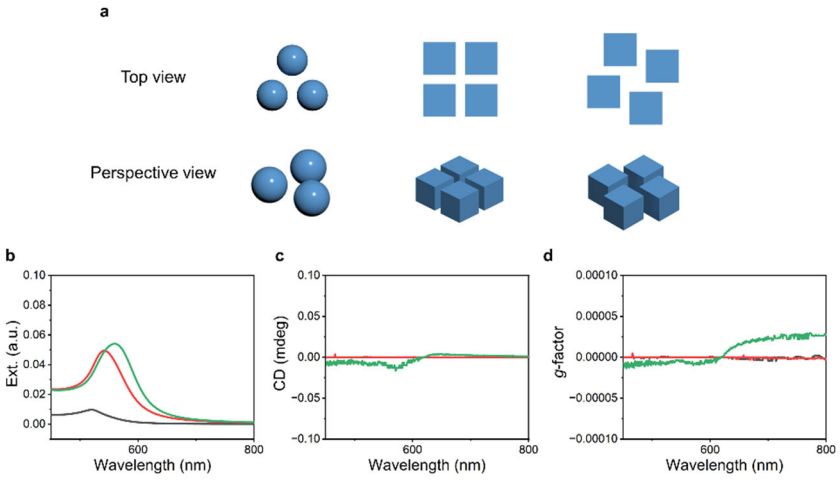

Supplementary Fig. 25. FDTD simulation for different nanoparticle assembly. (**a**) Schematics of the nanosphere and nanocube assemblies used in the FDTD simulation. The left two structures do not meet the symmetry requirement (i), and the right two structures meet both (i) and (ii). (**b**–**d**) Extinction, CD, and *g*-factor spectra of different assemblies: hexagonal lattice of nanospheres (black), square lattice of nanocubes (red), and twisted lattice of nanocubes (green). The results show that CD responses are only exhibited by structures that are lack of mirror symmetry and inversion symmetry due to the fixed structure orientation relative to the incident light. Details of the modelling can be found in Supplementary Note 5.

We revised the discussion on this new simulation in the conclusion part of the main text,

“These findings can be extended to a large library of achiral particles, their non-closely packed assemblies, and lattice reconfiguration pathways, which also allow for rich design space of metastructured surfaces with substrate-induced chiroptical activity (Supplementary Fig. 25).”

Reviewer Reports on the First Revision:

Referees' comments:

Referee #1 (Remarks to the Author):

The authors have adequately addressed my concerns and I would like to recommend it for publication in Nature.

Referee #2 (Remarks to the Author):

The authors have positively responded to the previous comments of all referees and adjusted the manuscript accordingly, which improved it. Also my comments are properly addressed and I am pleased to recommend it for publication in Nature. I am looking forward to seeing it in print!

Referee #3 (Remarks to the Author):

The authors have made significant amount of effort to improve the manuscript. All my questions are sufficiently answered, and my concerns are removed. I am happy to recommend for publication of the revised manuscript without further changes. Two minor comments:

1. I did not intend to ask the authors to provide direct evidence of spatial distribution for the two types of ligands on particle surface, but just to show the existence of both types of ligands in the purified sample (such as FTIR, NMR measurement results). I think that the thiol ligand control experiments that the authors provided are sufficient answer the question.

2. In the caption of Figure S25, I think the authors mean “the rightmost structure (twisted superlattice of nanocube) meets both (i) and (ii) symmetry requirements” but not “the right two structures”.

Author Rebuttals to First Revision:

Responses to Reviewers

Reviewer 1: *The authors have adequately addressed my concerns and I would like to recommend it for publication in Nature.*

Reply: We thank the reviewer for the positive feedback!

Reviewer 2: *The authors have positively responded to the previous comments of all referees and adjusted the manuscript accordingly, which improved it. Also my comments are properly addressed and I am pleased to recommend it for publication in Nature. I am looking forward to seeing it in print!*

Reply: We thank the reviewer for the positive feedback!

Reviewer 3: *The authors have made significant amount of effort to improve the manuscript. All my questions are sufficiently answered, and my concerns are removed. I am happy to recommend for publication of the revised manuscript without further changes.*

Reply: We thank the reviewer for the positive feedback and the clarification of previous comments!

Comment 1: *I did not intend to ask the authors to provide direct evidence of spatial distribution for the two types of ligands on particle surface, but just to show the existence of both types of ligands in the purified sample (such as FTIR, NMR measurement results). I think that the thiol ligand control experiments that the authors provided are sufficient answer the question.*

Reply: Thank you for the clarification! We are pleased that our zeta potential measurement and thiol ligand control experiments provided convincing evidence of the presence of two ligands on particle surface.

Comment 2: *In the caption of Figure S25, I think the authors mean "the rightmost structure (twisted superlattice of nanocube) meets both (i) and (ii) symmetry requirements" but not "the right two structures".*

Reply: We thank the reviewer for catching the typographical error! In the revised Supplementary Information, we have changed the caption of Supplementary Fig. 25 to "Schematics of the nanosphere and nanocube assemblies used in the FDTD simulation. The left two structures do not meet the symmetry requirement (i), and the rightmost structure meets both (i) and (ii)." based on the Reviewer's suggestion.